Scattering of fermions on a one-dimensional Q-ball

A.Yu. Loginov^a

^a Tomsk State University of Control Systems and Radioelectronics, 634050 Tomsk, Russia

Abstract

The scattering of massless fermions on a one-dimensional Q-ball is studied both analytically and numerically in the background field approximation. The wave functions of the fermionic scattering states are found in analytical form. General expressions are derived for the transmission and reflection coefficients and the corresponding S-matrix elements. General formulae describing the evaporation of the Noether charge of the one-dimensional Q-ball are given. A numerical study of the transmission and reflection coefficients along with the corresponding S-matrix elements is performed for a range of values of the model parameters. A study of the dependence of the evaporation rate of the Q-ball on the Yukawa coupling constant is carried out for several values of the Noether charge.

Keywords: Q-ball, Noether charge, fermion, Yukawa interaction *PACS:* 11.10.Lm, 11.27.+d, 11.80.-m

1. Introduction

Many field models possessing an unbroken global symmetry admit the existence of nontopological solitons [1, 2]. Nontopological solitons are spatially localized finite-energy solutions with topologically trivial field configurations. Unlike topological solitons [3, 4], which possess a nontrivial topology, topological triviality cannot ensure the stability of nontopological solitons. The main property of a nontopological soliton is that it is a local extremum (minimum or saddle point) of the energy functional for a fixed value of the conserved Noether charge. Under certain conditions, this extremum is an absolute minimum of the energy functional and the nontopological soliton is the ground state in the sector of a fixed Noether charge. In this case, the stability of the nontopological soliton is due to conservation of the Noether charge.

The simplest and most important nontopological soliton, proposed in Ref. [5] and known as the Q-ball [6], has been found in a U(1)-invariant model of a self-interacting complex scalar field. In Refs. [7, 8], it was shown that Q-balls can also exist in scalar field models possessing global non-Abelian symmetry. Furthermore, U(1) gauged models of complex self-interacting scalar fields also admit the existence of Q-balls [9–21]. In realistic models, Q-balls are generally allowed in supersymmetric extensions of the Standard Model that have flat directions in the interaction potential of scalar fields [22–24]. These Q-balls are of great interest to cosmological models describing the evolution of the early Universe [25–33]. In some models, Q-balls can survive to the present as places of concentration of dark matter [22, 26], whereas in other, Q-balls decay and do not survive to the present. In the latter case, Q-ball decay may result in the production of dark matter in the form of the lightest supersymmetric particles [27].

In realistic models, scalar fields forming a Q-ball interact with fermion fields. This interaction may have important consequences for the stability of the Q-ball [34, 35]. In particular, it was shown in Ref. [34] that the interaction of massless fermions with a scalar field leads to evaporation of the Q-ball. A numerical study of this process, taking into account real profiles of Q-ball solutions, was performed in Ref. [36]. A detailed study of the evaporation of a one-dimensional Q-ball was performed in Ref. [37], where the real profile of the Q-ball was approximated by a rectangular one.

Email address: a.yu.loginov@tusur.ru (A.Yu. Loginov)

Preprint submitted to Elsevier

Evaporation of the Q-ball is possible only within a limited range of the energy parameter. At larger values of the energy parameter, fermion-Q-ball scattering takes place rather than fermionic evaporation of the Q-ball. In the present work, we investigate the scattering of massless fermions on a one-dimensional Q-ball. We also investigate the fermionic evaporation of the Q-ball within an allowable region of the energy parameter. The choice of a one-dimensional Q-ball was made due to the fact that an analytical solution is known only for this case [1]. This makes it possible to obtain analytical expressions for the fermionic wave functions in the background field of the one-dimensional Q-ball. In turn, the analytical expressions of the fermionic wave functions allow us to obtain general expressions for the fermionic transmission and reflection coefficients, which considerably facilitates the study of fermion-Q-ball scattering.

This paper is structured as follows. In Sec. 2, we give a concise description of the Lagrangian, symmetries, and field equations of the model, and give the analytical form of a one-dimensional Q-ball solution. Section 3 presents an analytical description of fermion-Q-ball scattering. In particular, analytical expressions for the fermionic wave functions and general expressions for the transmission and reflection coefficients are presented. In Sec. 4, fermionic evaporation of the Q-ball is considered, and formulae describing this process are given. Section 5 contains numerical results. In particular, we discuss the dependence of the fermion transmission and reflection coefficients on an energy parameter. We also discuss the dependence of the evaporation rate of the Q-ball on the value of the Yukawa coupling constant. In the final section, we briefly summarise the results obtained in this work.

Throughout the paper, we use the natural units $\hbar = c = 1$.

2. Lagrangian and field equations of the model

The bosonic part of the model we are interested in has the Lagrangian density

$$\mathcal{L}_{\rm b} = \partial_{\mu}\phi\partial^{\mu}\phi^* - V\left(|\phi|\right),\tag{1}$$

where

$$V(|\phi|) = m^2 |\phi|^2 - \frac{g}{2} |\phi|^4 + \frac{h}{3} |\phi|^6$$
(2)

is the self-interaction potential of the complex scalar field ϕ . In Eq. (2), the coupling constants g and h are assumed to be positive and to satisfy the inequality $m^2hg^{-2} > 3/16$. It follows that the absolute minimum of the potential $V(|\phi|)$ occurs at $\phi = 0$, and the potential vanishes there.

The Lagrangian density (1) is invariant under the global U(1) transformations

$$\phi(t, x) \to \phi'(t, x) = \exp(-i\alpha) \phi(t, x).$$
(3)

We want to introduce fermions in such a way that the resulting model remains invariant under transformations (3). We also want the resulting model to have a conserved fermion current. To do this, we rewrite Eq. (1) in terms of the real and imaginary parts of the complex scalar field $\phi = 2^{-1/2} (\phi_1 + i\phi_2)$, where ϕ_1 and ϕ_2 are regarded as components of the scalar isotriplet $\phi = (\phi_1, \phi_2, 0)$ with a zero third component. We then introduce a fermionic isodublet ψ that interacts with the scalar isotriplet ϕ via the Yukawa interaction to obtain the Lagrangian density

$$\mathcal{L} = \frac{1}{2}\partial_{\mu}\phi \cdot \partial^{\mu}\phi - \frac{m^2}{2}\phi \cdot \phi + \frac{g}{8}\left(\phi \cdot \phi\right)^2 - \frac{h}{24}\left(\phi \cdot \phi\right)^3 + i\bar{\psi}\gamma^{\mu}\partial_{\mu}\psi - G\phi \cdot \bar{\psi}\boldsymbol{\tau}_{\perp}\psi, \tag{4}$$

where G is the Yukawa coupling constant, $\tau_{\perp} = (\tau_1, \tau_2)$, and $\tau_{1,2}$ are the corresponding Pauli matrices. In Eq. (4), the two indices of the Dirac field ψ_{ia} correspond to its spin-isospin structure. We use the following set of Dirac matrices in (1 + 1) dimensions:

$$\gamma^0 = \sigma_1, \ \gamma^1 = -i\sigma_2, \ \gamma_5 = \gamma^0\gamma^1 = \sigma_3, \tag{5}$$

where σ_k are the Pauli matrices. To distinguish the Pauli matrices σ_k acting on the spinor index *i* of the fermionic field ψ_{ia} from those acting on its isospinor index *a*, we denote the latter as τ_k .

The Lagrangian (4) depends on the four dimensional parameters: m, g, h, and G. By scaling the space-time coordinates, fields, and coupling constants as

$$x^{\mu} \to m^{-1} x^{\mu}, \ \phi \to m g^{-1/2} \phi, \ \psi \to m^{3/2} g^{-1/2} \psi, \ h \to m^{-2} g^2 h, \ G \to g^{1/2} G,$$
 (6)

the number of parameters of the Lagrangian (4) can be reduced to two. After scaling of Eq. (6), the Lagrangian (4) transforms as $\mathcal{L} \to m^4 g^{-1} \mathcal{L}_s$, where the scaled Lagrangian

$$\mathcal{L}_{\rm s} = \frac{1}{2}\partial_{\mu}\phi \cdot \partial^{\mu}\phi - \frac{1}{2}\phi \cdot \phi + \frac{1}{8}\left(\phi \cdot \phi\right)^{2} - \frac{h}{24}\left(\phi \cdot \phi\right)^{3} + i\bar{\psi}\gamma^{\mu}\partial_{\mu}\psi - G\phi \cdot \bar{\psi}\boldsymbol{\tau}_{\perp}\psi \tag{7}$$

depends only on the two parameters h and G. Note that the scaled fields and coupling constants included in Eq. (7) are dimensionless, as are the space-time coordinates on which these fields depend.

The Lagrangian (7) is invariant under the global transformations

$$\phi \rightarrow \phi' = \exp\left(-i\alpha T_3\right)\phi,$$
(8a)

$$\psi \rightarrow \psi' = \exp\left(-i\alpha t_3\right)\psi,$$
(8b)

where the generators $T_3 = -i\epsilon_{3ab}$ and $t_3 = \tau_3/2$. These transformations form the Abelian subgroup of the corresponding SU(2) group, and hence Eqs. (3) and (8a) are isomorphic. The invariance of the Lagrangian (7) under global transformations (8) results in the conserved Noether current

$$j_3^{\mu} = -\epsilon_{3ab} \left(\partial^{\mu} \phi_a\right) \phi_b + \frac{1}{2} \bar{\psi} \gamma^{\mu} \otimes \tau_3 \psi.$$
(9)

In addition to transformations (8), the Lagrangian (7) is also invariant under the global U(1) transformations

$$\psi \to \psi' = \exp\left(-i\beta\right)\psi,\tag{10}$$

resulting in the conserved fermion current

$$j_F^{\mu} = \bar{\psi}\gamma^{\mu} \otimes \mathbb{I}\psi. \tag{11}$$

The variation of the action $S = \int \mathcal{L} dx dt$ in the corresponding fields leads us to the field equations:

$$\partial_{\mu}\partial^{\mu}\phi + \phi - \frac{1}{2}\left(\phi \cdot \phi\right)\phi + \frac{h}{4}\left(\phi \cdot \phi\right)^{2}\phi + G\bar{\psi}\tau_{\perp}\psi = 0$$
(12)

and

$$i\gamma^{\mu}\partial_{\mu}\psi - G\,\phi\cdot\boldsymbol{\tau}_{\perp}\psi = 0. \tag{13}$$

It is known that under the condition h > 3/16, model (7) has a non-topological soliton solution called a Q-ball [6]. In the (1 + 1)-dimensional case, the Q-ball solution can be written in the analytical form:

$$\phi_1(t,x) = 2\sqrt{2\Omega} \left(1 + \kappa \cosh\left(2\Omega x\right)\right)^{-\frac{1}{2}} \cos\left(\omega t\right), \tag{14a}$$

$$\phi_2(t,x) = -2\sqrt{2}\Omega \left(1 + \kappa \cosh\left(2\Omega x\right)\right)^{-\frac{1}{2}} \sin\left(\omega t\right), \tag{14b}$$

$$\phi_3(t,x) = 0, \tag{14c}$$

where $\Omega = (1 - \omega^2)^{1/2}$ and $\kappa = (1 - (16/3) h\Omega^2)^{1/2}$. The parameter ω on which solution (14) depends is the phase frequency of the complex scalar field $\phi = 2^{-1/2}(\phi_1 + i\phi_2)$. The phase frequency of the Q-ball solution satisfies the condition $|\omega| \in (\omega_{\rm tn}, 1)$, where $\omega_{\rm tn} = (1 - 3/(16h))^{1/2}$. The main property of Q-ball solution (14) is that it is an absolute minimum of the energy functional in the sector of scalar field configurations with a fixed Noether charge $Q = \int j_3^0 dx$. It follows that Q-ball solution (14) is stable over the entire range of the parameter ω . As $|\omega| \to 1$, the energy and Noether charge of the one-dimensional Q-ball solution (14)

tend to zero as $E \sim |Q| \propto (1 - |\omega|)^{1/2}$. In contrast, as $|\omega| \to \omega_{\rm tn}$, the energy and Noether charge of the Q-ball diverge logarithmically as $E \sim \omega_{\rm tn} |Q| \propto -\ln (|\omega| - \omega_{\rm tn})$.

The Q-ball solution in Eq. (14) has the following symmetry properties under space and time reflections:

$$\phi_i(t, -x) = \phi_i(t, x), \qquad (15)$$

$$\phi_i(-t,x) = (-1)^{i+1} \phi_i(t,x), \qquad (16)$$

and, as a consequence of Eq. (16),

$$\boldsymbol{\phi}(t,x)\cdot\boldsymbol{\tau}_{\perp} = \boldsymbol{\phi}(-t,x)\cdot\boldsymbol{\tau}_{\perp}^{*}.$$
(17)

Using symmetry properties (15)–(17), it can easily be shown that if $\psi(t, x)$ is a solution to the Dirac equation (13) in the background field of Q-ball (14), then

$$\psi^{C}(t,x) = \eta_{C}\gamma_{5} \otimes \tau_{1}\psi^{*}(t,x), \qquad (18a)$$

$$\psi^{P}(t,x) = \eta_{P}\gamma^{0} \otimes \mathbb{I}\psi(t,-x), \qquad (18b)$$

$$\psi^{T}(t,x) = \eta_{T}\gamma^{0} \otimes \mathbb{I}\psi^{*}(-t,x)$$
(18c)

are also solutions to the Dirac equation (13) in the background field of the Q-ball, where η_C , η_P , and η_T are phase factors.

Under the reflection $\omega \to -\omega$, the energy $E(\omega)$ and Noether charge $Q(\omega)$ of Q-ball solution (14) are even and odd functions of ω , respectively. Using Eq. (17), it can be shown that if $\psi(t, x, \omega)$ is a solution to the Dirac equation in the background field of the Q-ball corresponding to the phase frequency ω , then

$$\psi(t, x, -\omega) = \mathbb{I} \otimes \tau_1 \psi(t, x, \omega) \tag{19}$$

is a solution to the Dirac equation in the background field of the Q-ball corresponding to the phase frequency $-\omega$. It follows that we can limit ourselves to studying the case of positive phase frequencies.

3. Scattering of fermions in the background field of the Q-ball

To obtain analytical expressions for the fermionic wave functions, we consider fermion-Q-ball scattering in the background field approximation, in which we neglect the fermion backreaction on the Q-ball field configuration. To allow us to neglect the fermion backreaction, the bosonic part of the non-scaled Lagrangian (4) should be much larger than the Yukawa term $G\phi \cdot \bar{\psi} \tau_{\perp} \psi$. To estimate these two values, we note that the magnitude of the scalar field of the Q-ball is $\propto m\Omega g^{-1/2}$, where $\Omega = (1 - \omega^2 m^{-2})^{1/2}$. Note that we return to the dimensional quantities in this and the following paragraph. We assume that the dimensionless combination m^2hg^{-2} is on the order of unity. It then follows that for fixed Ω , the contribution of the bosonic part of the Lagrangian (4) is $\propto m^2 g^{-1}$, whereas that of the Yukawa term is $\propto mg^{-1/2}$. Hence, the ratio of these contributions is $\propto mg^{-1/2}$, which may be much greater than unity for sufficiently small g. For small Ω , the bosonic part $\mathcal{L}_{\rm b} \approx 2^{-1}m^4\Omega^2 g^{-1}$, whereas the Yukawa term $\mathcal{L}_{\rm Yk} \approx mG\Omega L^{-1}g^{-1/2}$, where L is the normalised length of the fermion field. It follows that the background field approximation is invalid in the region of phase frequencies $m(1 - 2gm^{-6}G^2L^{-2}) \lesssim |\omega| < m$. This region can be made arbitrarily small if $g \ll 2^{-1}m^6G^{-2}L^2$; in this case, the region of non-applicability of the background field approximation corresponds to the so-called thick-wall regime [36, 38, 39] of the one-dimensional Q-ball.

We can see that for sufficiently small g, the background field approximation will be valid over the entire phase frequency range $|\omega| \in (\omega_{\rm tn}, m)$, except for a small region in the neighbourhood of $|\omega| = m$. From the viewpoint of QFT, however, we are talking about the scattering of a massless fermion of energy ε on a quantised Q-ball of mass $M_{\rm Qb}$. For the background field approximation to be valid, we must neglect the recoil of the Q-ball in this scattering. It follows that the fermion energy ε should be much less than the Q-ball mass $M_{\rm Qb}$. In the leading order in g, the Q-ball mass $M_{\rm Qb} \propto m^3 g^{-1}$, and hence the condition $\varepsilon \ll M_{\rm Qb}$ can be satisfied for sufficiently small gm^{-2} and fixed Ω . Although the Q-ball solution in Eq. (19) is time-dependent, it remains invariant under the combined action of the time translation and SO(2) rotation about the third isotopic axis:

$$\exp\left(-i\delta\omega T_{3}\right)\phi_{\mathrm{Ob}}\left(t+\delta,x\right) = \phi_{\mathrm{Ob}}\left(t,x\right),\tag{20}$$

where the generator $T_3 = -i\epsilon_{3ab}$. It follows that $\phi_{\rm Qb}(t, x)$ vanishes under the action of the operator $\partial_t - i\omega T_3$ in the same way as a time-independent field vanishes under the action of the time derivative ∂_t . Hence, in the background field of the Q-ball, fermionic wave functions are eigenfunctions of the operator $D_t = \partial_t - i\omega t_3$, where $t_3 = \tau_3/2$. Using the equation $iD_t\psi = \varepsilon\psi$, we obtain the time dependence of the components ψ_{ia} of the fermionic wave function

$$\psi = \begin{pmatrix} e^{-i\varepsilon - t}\psi_{11}\left(x\right) & e^{-i\varepsilon + t}\psi_{12}\left(x\right) \\ e^{-i\varepsilon - t}\psi_{21}\left(x\right) & e^{-i\varepsilon + t}\psi_{22}\left(x\right) \end{pmatrix},\tag{21}$$

where $\varepsilon_{\pm} = \varepsilon \pm \omega/2$. Substituting Eq. (21) into Eq. (13), we find that the Dirac equation splits into the two independent subsystems

$$i\begin{pmatrix}\psi_{11}\\\psi_{22}\end{pmatrix} = \begin{pmatrix}-\varepsilon_{-} & F(x)\\-F(x) & \varepsilon_{+}\end{pmatrix}\begin{pmatrix}\psi_{11}\\\psi_{22}\end{pmatrix}$$
(22)

and

$$i\begin{pmatrix}\psi_{12}\\\psi_{21}'\end{pmatrix} = \begin{pmatrix}-\varepsilon_{+} & F(x)\\-F(x) & \varepsilon_{-}\end{pmatrix}\begin{pmatrix}\psi_{12}\\\psi_{21}\end{pmatrix}.$$
(23)

In Eqs. (22) and (23), the function

$$F(x) = \frac{2^{3/2} G\Omega}{\sqrt{1 + \kappa \cosh\left(2\Omega x\right)}},\tag{24}$$

where the parameter $\kappa = \left(1 - (16/3) h\Omega^2\right)^{1/2}$.

The system (22) contains only the diagonal components ψ_{11} and ψ_{22} , whereas the system (23) contains only the antidiagonal components ψ_{12} and ψ_{21} . To explain this, we introduce the operator $T = \gamma_5 \otimes \tau_3$ and denote the diagonal and antidiagonal parts of the matrix ψ_{ia} as ψ_d and ψ_a , respectively:

$$\psi_{\rm d} = \begin{pmatrix} \psi_{11} & 0\\ 0 & \psi_{22} \end{pmatrix}, \quad \psi_{\rm a} = \begin{pmatrix} 0 & \psi_{12}\\ \psi_{21} & 0 \end{pmatrix}.$$
(25)

It is readily seen that

$$T\psi_{\rm d} = \psi_{\rm d}, \quad T\psi_{\rm a} = -\psi_{\rm a},$$
(26)

and hence ψ_d and ψ_a are the eigenmatrices of the operator T. At the same time, it can be shown that the operator T commutes with the Dirac Hamiltonian

$$H_D = \alpha \otimes \mathbb{I}(-i\partial_x) + G\beta \otimes \phi_{\mathrm{Ob}} \cdot \boldsymbol{\tau}_\perp, \tag{27}$$

where $\alpha = \gamma^0 \gamma^1 = \sigma_3$ and $\beta = \gamma^0 = \sigma_1$. It follows from this and Eq. (26) that the Hamiltonian H_D cannot mix ψ_d and ψ_a , and this results in the splitting of the Dirac equation into the two independent subsystems (22) and (23).

Eq. (18b) tells us that the parity transformation switches a diagonal fermionic state into an antidiagonal one:

$$\psi_{\rm d}\left(t,x\right) \xrightarrow{P} \psi_{\rm a}^{P}\left(t,x\right) = \eta_{P}\gamma^{0} \otimes \mathbb{I}\psi_{\rm d}\left(t,-x\right).$$
⁽²⁸⁾

It follows from Eq. (28) that for given values of ε and ω , the diagonal and antidiagonal fermionic states are connected to each other via the unitary *P*-transformation. The unitary *P*-transformation keeps the magnitudes of the incident, transmitted, and reflected fermionic fluxes unchanged. Hence, the reflection and transmission coefficients do not change when passing from the diagonal to antidiagonal states. Next, let us denote the transformation in Eq. (19) by the symbol *R*. The *R* transformation changes the sign of the phase frequency ω and transforms a diagonal (antidiagonal) fermionic state to an antidiagonal (diagonal) one:

$$\psi_{\mathbf{d},\mathbf{a}}\left(t,x,-\omega\right) \xrightarrow{R} \psi_{\mathbf{a},\mathbf{d}}^{R}\left(t,x,\omega\right) = \mathbb{I} \otimes \tau_{1}\psi_{\mathbf{d},\mathbf{a}}\left(t,x,-\omega\right).$$
⁽²⁹⁾

We see that the diagonal (antidiagonal) fermionic states corresponding to the phase frequency $-\omega$ are unitarily equivalent to the antidiagonal (diagonal) fermionic states corresponding to the phase frequency ω . As in the previous case, unitary transformation (29) keeps the magnitudes of the incident, transmitted, and reflected fermionic fluxes unchanged, and hence cannot change the reflection and transmission coefficients. It follows from the above that in the study of fermion-Q-ball scattering, it is sufficient to limit ourselves to the case of positive ω and diagonal fermionic states.

The system (22) describes the scattering of the diagonal fermionic states ψ_d . It can be shown that it is equivalent to the second-order differential equation

$$\psi_{11}''(x) + \left(i\omega + \frac{\kappa\Omega\sinh\left(2\Omega x\right)}{1 + \kappa\cosh\left(2\Omega x\right)}\right)\psi_{11}'(x) + \left(\varepsilon_{-}\varepsilon_{+} - \frac{\Omega\left(8G^{2}\Omega + i\varepsilon_{-}\kappa\sinh\left(2\Omega x\right)\right)}{1 + \kappa\cosh\left(2\Omega x\right)}\right)\psi_{11}(x) = 0$$
(30)

together with the differential relation

$$\psi_{22}(x) = F(x)^{-1} \left(i\psi_{11}'(x) + \varepsilon_{-}\psi_{11}(x) \right).$$
(31)

The structure of Eq. (30) becomes clearer if we eliminate the hyperbolic functions. In order to do this, we change to a new independent variable

$$\xi = \frac{1}{2} \frac{\left(\sqrt{1-\kappa} + \sqrt{1+\kappa}\right) \left(1 - \tanh\left(\Omega x\right)\right)}{\sqrt{1+\kappa} - \sqrt{1-\kappa} \tanh\left(\Omega x\right)}.$$
(32)

Written in terms of this new variable ξ , Eq. (30) takes the form

$$\psi_{11}''(\xi) + \frac{1}{2} \left(\frac{1}{\xi - a} + \frac{\Omega - i\omega}{\Omega\xi} + \frac{\Omega + i\omega}{\Omega(\xi - 1)} \right) \psi_{11}'(\xi) + \frac{1}{4\Omega(\xi - 1)\xi} \left(\frac{8(1 - 2a)G^2\Omega - i\varepsilon_-}{\xi - a} - \frac{\varepsilon_-(\varepsilon_+ - i\Omega)}{\Omega\xi} + \frac{\varepsilon_-(\varepsilon_+ + i\Omega)}{\Omega(\xi - 1)} \right) \psi_{11}(\xi) = 0,$$
(33)

where the parameter

$$a = \frac{1}{2} \left(1 + \left(1 - \kappa^2 \right)^{-1/2} \right) = \frac{1}{2} + \frac{\sqrt{3}}{8\sqrt{h\Omega}}.$$
 (34)

Eq. (33) has four regular singularities located at the points $\xi = 0$, $\xi = 1$, $\xi = a$, and $\xi = \infty$. It follows that in the neighbourhoods of these points, the solution to Eq. (33) can be expressed in terms of the local Heun functions [40, 41].

Using Eqs. (30) and (31), it can easily be shown that the component $\psi_{11}(t,x) \propto \exp(-i\varepsilon_-(t-x))$ as $x \to \pm \infty$. At the same time, the component $\psi_{22}(t,x) \propto \exp(-i\varepsilon_+(t+x))$ as $x \to \pm \infty$. It follows that far from the Q-ball, the component ψ_{11} corresponds to a right-chiral massless fermion moving to the right, whereas the component ψ_{22} corresponds to a left-chiral massless fermion moving to the left. Let the right-moving fermionic wave ψ_{11} fall on the Q-ball from the left. The fermion-Q-ball interaction results in the transmitted right-moving fermionic wave ψ_{11} as $x \to +\infty$, and the reflected left-moving fermionic wave ψ_{22} as $x \to -\infty$.

The solution to Eq. (33) corresponding to the transmitted fermionic wave is

$$\psi_{11}(\xi) = (1-\xi)^{\frac{i\varepsilon_{-}}{2\Omega}} (a-\xi)^{\frac{1}{2}} \xi^{-\frac{i\varepsilon_{-}}{2\Omega}} Hl[a, q_{\rm tr}, \alpha_{\rm tr}, \beta_{\rm tr}, \gamma_{\rm tr}, \delta_{\rm tr}, \xi], \qquad (35)$$

where the parameters

$$\alpha_{\rm tr} = 1, \tag{36a}$$

$$\beta_{\rm tr} = \frac{1}{2}, \tag{36b}$$

$$\gamma_{\rm tr} = \frac{1}{2} - \frac{i}{2} \frac{\varepsilon_+ + \varepsilon_-}{\Omega}, \qquad (36c)$$

$$\delta_{\rm tr} = \frac{1}{2} + \frac{i}{2} \frac{\varepsilon_+ + \varepsilon_-}{\Omega}, \qquad (36d)$$

$$q_{\rm tr} = \frac{1}{4} + 2(2a-1)G^2 - \frac{i}{4}\frac{\varepsilon_+ + \varepsilon_-}{\Omega},$$
 (36e)

and we use the notation $Hl(a, q; \alpha, \beta, \gamma, \delta; \xi)$ for the six-parameter local Heun function [40, 41]. Turning to the variable x and using the properties of the local Heun function [40, 41], we obtain the leading term of the asymptotics of the transmitted fermionic wave as

$$\psi_{11}(x) \sim a^{\frac{1}{2}} e^{\frac{i\varepsilon_{-}}{4\Omega} \ln\left(1 - \frac{1}{a}\right)} e^{i\varepsilon_{-}x}$$
(37)

as $x \to +\infty$.

The local Heun function $Hl(a, q; \alpha, \beta, \gamma, \delta; \xi)$ is analytic, and is equal to one at the regular singular point $\xi = 0$. Hence, it can be expanded in a Taylor series about this point. In the complex ξ -plane, the radius of convergence of this series is equal to min (1, a) = 1, as it follows from Eq. (34) that a > 1. In this case, the local Heun function $Hl(a, q; \alpha, \beta, \gamma, \delta; \xi)$ can be analytically continued from the unit disk to the whole complex plane with the branch cut discontinuity $[1, \infty)$, and its values are indeterminate at the regular singular points $\xi = 1$ and $\xi = a$. It also follows from Eq. (32) that $\xi \to 1$ as $x \to -\infty$. Hence, we cannot use Eq. (35) to describe the incident fermionic wave far to the left of the Q-ball.

To describe the incident fermionic wave, we must use the local Heun functions, which are well-defined at the point $\xi = 1$. Knowing the prefactor (the product of the first three factors in Eq. (35)) and parameters (36), and using the symmetry properties of Heun's equation [40, 41], we can write the general form of the local solution to Eq. (33) in the neighbourhood of $\xi = 1$ as

$$\psi_{11}(\xi) = c_1 (1-\xi)^{\frac{i\varepsilon_{-}}{2\Omega}} (a-\xi)^{\frac{1}{2}} \xi^{-\frac{i\varepsilon_{-}}{2\Omega}} Hl [1-a, q_{\rm in}, \alpha_{\rm in}, \beta_{\rm in}, \gamma_{\rm in}, \delta_{\rm in}, 1-\xi] + c_2 (1-\xi)^{\frac{1}{2} - \frac{i\varepsilon_{+}}{2\Omega}} (a-\xi)^{\frac{1}{2}} \xi^{-\frac{i\varepsilon_{-}}{2\Omega}} Hl [1-a, q_{\rm rf}, \alpha_{\rm rf}, \beta_{\rm rf}, \gamma_{\rm rf}, \delta_{\rm rf}, 1-\xi],$$
(38)

where the parameters

$$\alpha_{\rm in} = 1, \tag{39a}$$

$$\beta_{\rm in} = \frac{1}{2}, \tag{39b}$$

$$\gamma_{\rm in} = \frac{1}{2} + \frac{i}{2} \frac{\varepsilon_+ + \varepsilon_-}{\Omega}, \qquad (39c)$$

$$\delta_{\rm in} = \frac{1}{2} - \frac{i}{2} \frac{\varepsilon_{\pm} + \varepsilon_{-}}{\Omega}, \qquad (39d)$$

$$q_{\rm in} = \frac{1}{2} - q_{\rm tr},$$
 (39e)

and

$$\alpha_{\rm rf} = \frac{3}{2} - \frac{i}{2} \frac{\varepsilon_+ + \varepsilon_-}{\Omega}, \qquad (40a)$$

$$\beta_{\rm rf} = 1 - \frac{i}{2} \frac{\varepsilon_+ + \varepsilon_-}{\Omega}, \qquad (40b)$$

$$\gamma_{\rm rf} = \frac{3}{2} - \frac{i}{2} \frac{\varepsilon_+ + \varepsilon_-}{\Omega}, \qquad (40c)$$

$$\delta_{\rm rf} = \frac{1}{2} - \frac{i}{2} \frac{\varepsilon_+ + \varepsilon_-}{\Omega}, \qquad (40d)$$

$$q_{\rm rf} = \frac{6-a}{4} + \frac{(a-1)(\varepsilon_+ + \varepsilon_-)^2}{4\Omega^2} + i\frac{(2a-5)(\varepsilon_+ + \varepsilon_-)}{4\Omega} - q_{\rm tr}.$$
(40e)

The solutions in Eqs. (35) and (38) have a common domain of analyticity. To determine the coefficients c_1 and c_2 in Eq. (38), we need to equate Eqs. (35) and (38) as well as their derivatives in ξ at any point in their common domain of analyticity; the values of the coefficients will not depend on the specific choice of

this point. To simplify the formulae, we choose the symmetric point $\xi = 1/2$ as the matching point. As a result, we obtain the following expressions for the coefficients c_1 and c_2 :

$$c_{1} = \frac{\chi_{\rm tr}(1/2)}{\chi_{\rm in}(1/2)} - \Omega \frac{\chi_{\rm rf}(1/2) W_{\rm ti}(1/2)}{\chi_{\rm in}(1/2) V(1/2)},\tag{41}$$

$$c_{2} = 2^{\frac{1}{2} - \frac{i}{2} \frac{\varepsilon_{+} + \varepsilon_{-}}{\Omega}} \Omega \frac{W_{\text{ti}}(1/2)}{V(1/2)}, \qquad (42)$$

where the functions

$$\chi_{\rm in}\left(\xi\right) = Hl\left[1-a, q_{\rm in}, \alpha_{\rm in}, \beta_{\rm in}, \gamma_{\rm in}, \delta_{\rm in}, 1-\xi\right],\tag{43a}$$

$$\chi_{\rm rf}(\xi) = Hl \left[1 - a, q_{\rm rf}, \alpha_{\rm rf}, \beta_{\rm rf}, \gamma_{\rm rf}, \delta_{\rm rf}, 1 - \xi\right], \tag{43b}$$

$$\chi_{\rm tr}\left(\xi\right) = Hl\left[a, q_{\rm tr}, \alpha_{\rm tr}, \beta_{\rm tr}, \gamma_{\rm tr}, \delta_{\rm tr}, \xi\right],\tag{43c}$$

the Wronskians

$$W_{\rm ri}\left(\xi\right) = \chi_{\rm rf}\left(\xi\right)\chi_{\rm in}'\left(\xi\right) - \chi_{\rm rf}'\left(\xi\right)\chi_{\rm in}\left(\xi\right),\tag{44a}$$

$$W_{\rm ti}(\xi) = \chi_{\rm tr}(\xi) \chi'_{\rm in}(\xi) - \chi'_{\rm tr}(\xi) \chi_{\rm in}(\xi), \qquad (44b)$$

and the combination

$$V(\xi) = \Omega W_{\rm ri}(\xi) + (\Omega - i(\varepsilon_+ + \varepsilon_-))\chi_{\rm in}(\xi)\chi_{\rm rf}(\xi).$$
(45)

As $x \to -\infty$, the asymptotics of ψ_{11} takes the form

$$\psi_{11} \sim c_1 \left(a - 1\right)^{\frac{1}{2}} e^{\frac{i\varepsilon_-}{4\Omega} \ln\left(1 - \frac{1}{a}\right)} e^{i\varepsilon_- x} + c_2 \left(a - 1\right)^{\frac{3}{4}} a^{-\frac{1}{4}} e^{-\frac{i\varepsilon_+}{4\Omega} \ln\left(1 - \frac{1}{a}\right)} e^{\Omega x} e^{-i\varepsilon_+ x}.$$
(46)

We see that as $x \to -\infty$, ψ_{11} is the sum of the right-moving wave that is $\propto c_1$ (the incident fermionic wave) and the exponentially damped wave that is $\propto c_2$. Using Eqs. (31) and (46), we can ascertain the asymptotic behaviour of the ψ_{22} component as $x \to -\infty$ as follows:

$$\psi_{22} \sim \frac{c_2}{2^{3/2}G} \frac{a-1}{(2a-1)^{1/2}} \frac{\varepsilon_+ + \varepsilon_- + i\Omega}{\Omega} e^{-\frac{i\varepsilon_+}{4\Omega} \ln(1-a^{-1})} e^{-i\varepsilon_+ x}.$$
(47)

We see that as $x \to -\infty$, ψ_{22} is the left-moving wave (the reflected fermionic wave) which is $\propto c_2$.

In the background field of the Q-ball, fermions become asymptotically free and massless as $x \to \pm \infty$. The free massless fermions can be characterised by their energy ε_{\pm} , isospin projection I_3 , and chirality ± 1 . Using Dirac's notations, we denote the asymptotic states of the incident, transmitted and reflected fermions as $|\varepsilon_{-}, 1/2, R\rangle^{(\text{in})}$, $|\varepsilon_{-}, 1/2, R\rangle^{(\text{out})}$, and $|\varepsilon_{+}, -1/2, L\rangle^{(\text{out})}$, respectively, where R(L) denotes positive (negative) chirality. Following the standard method of scattering theory [42–44], we shall use the S operator to describe the fermion-Q-ball scattering. Acting on the state $|\varepsilon_{-}, 1/2, R\rangle^{(\text{in})}$, the S operator turns it into a linear combination of the states $|\varepsilon_{-}, 1/2, R\rangle^{(\text{out})}$ and $|\varepsilon_{+}, -1/2, L\rangle^{(\text{out})}$:

$$S |\varepsilon_{-}, 1/2, R\rangle^{(\text{in})} = S_{1/2, 1/2} |\varepsilon_{-}, 1/2, R\rangle^{(\text{out})} + S_{-1/2, 1/2} |\varepsilon_{+}, -1/2, L\rangle^{(\text{out})},$$
(48)

where the S-matrix elements

$$S_{1/2,1/2} = {}^{(\text{out})} \langle \varepsilon_{-}, 1/2, R | S | \varepsilon_{-}, 1/2, R \rangle^{(\text{in})}, \qquad (49a)$$

$$S_{-1/2,1/2} = {}^{(\text{out})} \langle \varepsilon_+, -1/2, L | S | \varepsilon_-, 1/2, R \rangle^{(\text{in})} .$$
(49b)

Using asymptotic forms (37), (46), and (47), we can write the S-matrix elements included in Eq. (48) as

$$S_{1/2,1/2} = \left(1 - a^{-1}\right)^{-1/2} c_1^{-1} \tag{50}$$

and

$$S_{-1/2,1/2} = 2^{-3/2} c_2 c_1^{-1} G^{-1} \left(\frac{a-1}{2a-1}\right)^{1/2} \left(2\varepsilon \Omega^{-1} + i\right) e^{-i\frac{\varepsilon}{2\Omega}\ln\left(1-a^{-1}\right)}.$$
(51)

The S-matrix elements (50) and (51) satisfy the unitarity condition

$$|S_{-1/2,1/2}|^2 + |S_{1/2,1/2}|^2 = 1.$$
 (52)

Substituting asymptotic forms (37), (46), and (47) into the expression for the spatial component of the fermion current given in Eq. (11), we can calculate the transmission and reflection coefficients:

$$T = \frac{j_{\rm tr}}{j_{\rm in}} = |c_1|^{-2} \frac{a}{a-1}$$
(53)

and

$$R = \frac{|j_{\rm rf}|}{j_{\rm in}} = \frac{|c_2|^2}{|c_1|^2} \frac{1}{8G^2} \frac{a-1}{2a-1} \left(1 + 4\varepsilon^2 \Omega^{-2}\right).$$
(54)

It follows from Eqs. (50), (51), (53), and (54) that the transmission and reflection coefficients are the squared magnitudes of the corresponding S-matrix elements:

$$T = |S_{1/2,1/2}|^2$$
 and $R = |S_{-1/2,1/2}|^2$. (55)

Eqs. (52) and (55) then tell us that for given values of ω and ε (recall that $\varepsilon = \varepsilon_{\pm} \mp \omega/2$), the transmission and reflection coefficients satisfy the unitarity condition

$$T(\varepsilon,\omega) + R(\varepsilon,\omega) = 1.$$
(56)

In the process of scattering, the transmitted fermionic wave acquires a phase shift δ with respect to the incident fermionic wave. From Eqs. (37), (46), and (50) it follows that

$$\delta(\varepsilon,\omega) = -\arg\left[c_1(\varepsilon,\omega)\right] = \arg\left[S_{1/2,1/2}(\varepsilon,\omega)\right].$$
(57)

Eqs. (46) and (47) tell us that there are no bound diagonal fermionic states ψ_d in the background field of the Q-ball. This is because there are no diagonal fermionic states for which both the ψ_{11} and ψ_{22} components decrease exponentially as $x \to \pm \infty$. A similar situation occurs for the antidiagonal fermionic states ψ_a . In the model under consideration, fermions acquire mass only through the Yukawa interaction. As $x \to \pm \infty$, the Q-ball's field $\phi_{\rm Qb}$ tends to zero exponentially, and thus fermions become asymptotically massless. The absence of a mass gap in the spectrum of the Dirac Hamiltonian makes it impossible for fermionic bound states to exist in the background field of the Q-ball.

4. Evaporation of the Q-ball

It was shown in Ref. [34] that the Yukawa interaction of the scalar field of a Q-ball with massless fermions leads to evaporation of the Q-ball. In our case, this means that the energy and Noether charge of the Q-ball are carried away by a flux of fermion-antifermion pairs. The evaporation of the Q-ball is possible only when the energy parameter $\varepsilon \in (-\omega/2, \omega/2)$. In this case, the parameter $\varepsilon_{-} = \varepsilon - \omega/2$ becomes negative, and therefore in Eq. (21), the components ψ_{11} and ψ_{21} correspond to antifermionic states.

As $\omega \to \omega_{\rm tn}$, the Q-ball passes into the thin-wall regime. In this regime, the energy, Noether charge, and spatial size of the one-dimensional Q-ball increase indefinitely in the limit of $\omega \to \omega_{\rm tn}$, and the energy and charge densities become spatially homogeneous within the Q-ball, except for two thin boundary transition layers. It was shown in Ref. [34] that in the thin-wall regime, the production of pairs cannot occur in the interior of the Q-ball, but only in the thin transition layer at its boundary. In our case, this is because the scalar-fermion Yukawa interaction shifts the point to which we fill the Dirac sea. Specifically, for the components ψ_{12} and ψ_{22} , the Dirac sea is filled to the level $\omega/2$ and is overflowed. In contrast, for the components ψ_{11} and ψ_{21} , the Dirac sea is filled to the level $-\omega/2$ and is underflowed. As a result, no fermion-antifermion pairs with a total energy of ω can be produced in the interior of the Q-ball, and evaporation becomes impossible there.

However, evaporation is possible in the thin transition layer at the Q-ball boundary. In Ref. [34], the evaporation rate was calculated based on a leading order semi-classical approximation, in which massless fermions were considered in the presence of the classical background field of a Q-ball. A detailed derivation of the evaporation rate for the one-dimensional case is given in Ref. [37]. In our case, the evaporation rate of the Q-ball is

$$\frac{dQ}{dt} = \frac{2}{\pi}m \int_{0}^{\frac{\tilde{\omega}}{2}} R(\tilde{\varepsilon}, \tilde{\omega}, \tilde{h}, \tilde{G}) d\tilde{\varepsilon},$$
(58)

where R is the reflection coefficient and m is the mass of the scalar field ϕ . In the discussion in this section, the dimensionless parameters (defined by Eq. (6)) are marked with a tilde, so that the dimensionless arguments of R are $\tilde{\varepsilon} = m^{-1}\varepsilon$, $\tilde{\omega} = m^{-1}\omega$, $\tilde{h} = m^2 g^{-2}h$, and $\tilde{G} = g^{-1/2}G$. In Eq. (58), the reflection coefficient R is calculated using the general formulae in Sec. 3. Using the relation $dE/dQ = \omega$, we can also calculate the rate of energy loss of the Q-ball

$$\frac{dE}{dt} = \frac{dE}{dQ}\frac{dQ}{dt} = \omega\frac{dQ}{dt} = \frac{2}{\pi}\omega m \int_{0}^{\frac{\omega}{2}} R(\tilde{\varepsilon}, \tilde{\omega}, \tilde{h}, \tilde{G})d\tilde{\varepsilon}.$$
(59)

Using the inequality R < 1, which follows from the unitarity condition (56), we obtain the upper bound on the evaporation rate of the Noether charge of the Q-ball

$$\left. \frac{dQ}{dt} \right|_{\max} = \frac{\omega}{\pi} \approx \frac{\omega_{\rm tn}}{\pi} = \frac{m}{\pi} \left[1 - (3/16) \left(m^2 h g^{-2} \right)^{-1} \right]^{1/2},\tag{60}$$

where we use the fact that $\omega \approx \omega_{\rm tn}$ in the thin-wall regime. It is important to note that this upper bound does not depend on the Yukawa coupling constant G, and is determined only by the parameters of the bosonic sector of model (4). The combination of Eqs. (59) and (60) gives us the upper bound on the rate of energy loss of the Q-ball

$$\left. \frac{dE}{dt} \right|_{\max} = \frac{\omega^2}{\pi} \approx \frac{\omega_{\rm tn}^2}{\pi} = \frac{m^2}{\pi} \left[1 - (3/16) \left(m^2 h g^{-2} \right)^{-1} \right]. \tag{61}$$

In the thin-wall regime, the energy and Noether charge densities are approximately constant in the interior of the Q-ball. In this regime, the magnitude of the Noether charge density is

$$j_0 \approx \frac{3}{2} \frac{mg}{h} \left(1 - \frac{3}{16} \frac{g^2}{m^2 h} \right)^{1/2}.$$
 (62)

It follows that in the thin-wall regime, the magnitude of the Noether charge of the Q-ball is

$$Q \approx j_0 L,\tag{63}$$

where L is the linear size of the one-dimensional Q-ball. Using Eqs. (58), (62), and (63), we can find the velocity of recession of L as a result of Q-ball evaporation as follows:

$$\frac{dL}{dt} = \frac{1}{j_0} \frac{dQ}{dt} = \frac{2}{3} \frac{h}{g} \left(1 - \frac{3}{16} \frac{g^2}{m^2 h} \right)^{-1/2} \frac{2}{\pi} \int_0^{\frac{\omega}{2}} R\left(\tilde{\varepsilon}, \tilde{\omega}, \tilde{h}, \tilde{G}\right) d\tilde{\varepsilon}.$$
(64)

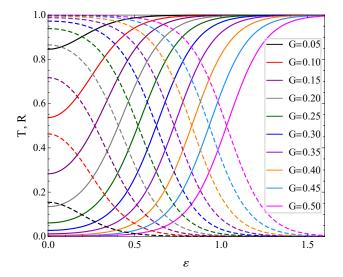


Fig. 1. Dependence of the transmission coefficient T (solid curves) and reflection coefficient R (dashed curves) on the energy parameter ε for different values of the Yukawa coupling constant G. The curves correspond to the parameters h = 0.2 and $\omega = 0.5$.

From Eqs. (56) and (64) it follows that the upper bound on dL/dt is

$$\left. \frac{dL}{dt} \right|_{\max} \approx \frac{2}{3\pi} \frac{h}{g} = \frac{2h}{3\pi} \frac{g}{m^2}.$$
(65)

All of the formulae in this section were derived in the leading (one-loop) order of the semi-classical approximation, which is valid in the limit of small \hbar . In this paper, however, we use the natural units $\hbar = c = 1$. It can be shown [1] that in this case, the semi-classical limit is the limit of small gm^{-2} , where the remaining dimensionless combinations $\tilde{\omega} = \omega/m$, $\tilde{h} = m^2 g^{-2} h$, and $\tilde{G} = g^{-1/2} G$ are fixed and are $\lesssim 1$. This is because after scaling as in Eq. (6), the action $S_T = \int_0^{\frac{2\pi}{\omega}} \int_{-\infty}^{+\infty} \mathcal{L} dx dt$ over the period $T = 2\pi/\omega$ is scaled as

$$S_T(\omega, m, g, h, G) \to m^2 g^{-1} S_T(\tilde{\omega}, 1, 1, \tilde{h}, \tilde{G}).$$

$$(66)$$

It follows that as $m^2 g^{-1} \to \infty$, the contribution of arbitrary field configurations to the functional integrals of QFT will be strongly suppressed, due to fast oscillations in the exponential factor exp $[im^2g^{-1}S_T]$. In this case, the main contribution to the functional integrals comes from field configurations in infinitesimal neighbourhoods of the classical solutions (stationary points of action), which is the main feature of the semi-classical regime.

As noted above, the existence of the Q-ball is only possible if $\tilde{h} = m^2 g^{-2} h > 3/16$. On the other hand, we assume that the dimensionless constant \tilde{h} must be on the order of or less than unity for the model to be consistent from the viewpoint of QFT. Eq. (65) then tells us that in the semi-classical limit of small gm^{-2} , the velocity dL/dt is much smaller than the speed of light c = 1.

5. Numerical results

The Dirac equation (13), when written in terms of dimensionless quantities (6), depends on the three dimensionless parameters h, G, and ω . Our main goal is to ascertain the dependence of the fermion-Q-ball scattering on the Yukawa coupling constant G and phase frequency ω . For this reason, we fix the nonlinear coupling constant h to 0.2. At this value of h, the magnitude of the phase frequency of the Q-ball can vary in a comparatively wide range (0.25, 1).

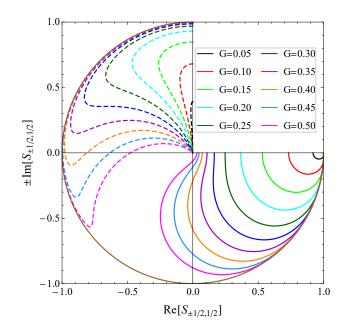


Fig. 2. Argand diagram for the S-matrix elements $S_{1/2, 1/2}$ (solid curves) and the complex conjugate S-matrix elements $S^*_{-1/2, 1/2}$ (dashed curves) for different values of the Yukawa coupling constant G. The curves correspond to the parameters h = 0.2 and $\omega = 0.5$.

Figure 1 illustrates the dependence of the transmission coefficient T and reflection coefficient R on the energy parameter $\varepsilon = (\varepsilon_+ + \varepsilon_-)/2$ for h = 0.2, $\omega = 0.5$, and different values of the Yukawa coupling constant G. It follows from Fig. 1 that $T(\varepsilon)$ and $R(\varepsilon)$ are even functions of ε . This symmetry property is a consequence of the invariance of the Dirac equation (13) under the C-conjugation (18a). In Fig. 1, the curves $T(\varepsilon)$ and $R(\varepsilon)$ corresponding to the same value of G satisfy the unitarity condition (56). Another characteristic property is that for nonzero G, the curves $T(\varepsilon)$ do not vanish at $\varepsilon = 0$. Accordingly, the curves $R(\varepsilon)$ are different from unity at $\varepsilon = 0$ and nonzero G. This property is a consequence of the non-trivial time dependence of the Q-ball solution in Eq. (14), which results in the nonconservation of energy in fermion-Q-ball scattering. We find that for sufficiently large G, the value of T(0) tends to zero exponentially with increasing G. Accordingly, the value of R(0) tends to unity exponentially in this regime. As $G \to 0$, the value of R(0) (T(0)) tends to zero (unity) $\propto G^2$.

Let us define the parameter $\varepsilon_{1/2}$ by the condition $T(\varepsilon_{1/2}) = R(\varepsilon_{1/2}) = 1/2$. We also determine the effective Yukawa mass of the fermion in the background field of the Q-ball as follows:

$$m_{\psi,\text{eff}} = G \left| \phi\left(0\right) \right| = 2^{3/2} G \Omega \left[1 + \left(1 - 16h\Omega^2/3\right)^{1/2} \right]^{-1/2}, \tag{67}$$

where $\Omega = (1 - \omega^2)^{1/2}$. We then find that in Fig. 1, the parameter $\varepsilon_{1/2}$ satisfies the approximate relation

$$\varepsilon_{1/2} \approx m_{\psi,\text{eff}}$$
 (68)

for the curves $T(\varepsilon)$ and $R(\varepsilon)$, such that $T(0) \ll 1$ and $1 - R(0) \ll 1$, respectively. In particular, the parameter $\varepsilon_{1/2}$ is approximately $\propto G$ for these curves.

Figure 2 presents an Argand diagram for the elastic S-matrix elements $S_{1/2, 1/2}$ and the complex conjugate inelastic S-matrix elements $S_{-1/2, 1/2}^*$ for different values of the Yukawa coupling constant G. We present the conjugate S-matrix elements $S_{-1/2, 1/2}^*$ rather than $S_{-1/2, 1/2}$ in order to avoid intersection between the solid and dashed curves. It follows from Fig. 2 that for $\varepsilon = 0$, the elastic S-matrix elements $S_{1/2, 1/2}$ are real. They tend to unity as $G \to 0$, and to zero with an increase in G. As ε increases, the matrix elements $S_{1/2, 1/2}$ leave the real axis and move along the solid curves in Fig. 2. With a further rise in ε , they approach

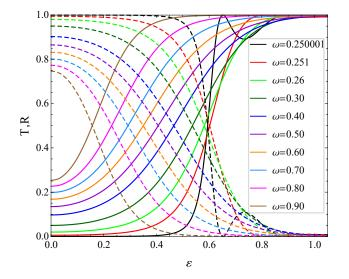


Fig. 3. Dependence of the transmission coefficient T on the energy parameter ε for different values of the phase frequency of the Q-ball. The curves correspond to the parameters h = 0.2 and G = 0.2.

the unitary circle and then tend to unity as $\varepsilon \to \infty$. It follows that when G is fixed and $\varepsilon \to \infty$, the fermion-Q-ball interaction becomes negligibly small.

The behaviour of the curves corresponding to the elastic matrix elements $S_{1/2, 1/2}$ and Eq. (57) tell us that the phase shifts $\delta(\varepsilon)$ tend to zero for both $\varepsilon \to 0$ and $\varepsilon \to \infty$. In particular, it was found that the phase shifts $\delta(\varepsilon)$ tend to zero $\propto \varepsilon^{-1}$ as $\varepsilon \to \infty$. Hence, the differences in the phase shifts $\Delta = \delta(0) - \delta(\infty)$ of the elastic matrix elements $S_{1/2, 1/2}$ are equal to zero for all values of the Yukawa coupling constant G.

In contrast to $S_{1/2, 1/2}$, the inelastic S-matrix elements $S_{-1/2, 1/2}$ are purely imaginary when $\varepsilon = 0$; they tend to zero as $G \to 0$ and to -i as G increases. As ε increases, the matrix elements $S_{-1/2, 1/2}$ leave the imaginary axis and move along the dashed curves in Fig. 2. For sufficiently large G and sufficiently small ε , the dashed curves are close to the unitary circle. With a further rise in ε , the dashed curves tend to the origin, indicating the exponential suppression of the fermion reflection as $\varepsilon \to \infty$.

Next, we investigate the dependence of fermion-Q-ball scattering on the phase frequency ω for fixed values of the other model parameters. Figure 3 shows the dependence of the transmission coefficient T and reflection coefficient R on the energy parameter $\varepsilon = (\varepsilon_+ + \varepsilon_-)/2$ for h = 0.2, G = 0.2, and different values of the phase frequency ω . In the same way as in Fig. 1, we see that the curves $T(\varepsilon)$ and $R(\varepsilon)$ are even functions of ε , and the values of T(0) (R(0)) are different from zero (unity). However, the value of T(0) (R(0)) tends to zero (unity) in the thin-wall regime when $\omega \to \omega_{\rm tn} = 1/4$. In Fig. 3, the positions of the intersection points of the corresponding curves $T(\varepsilon)$ and $R(\varepsilon)$ are reasonably well defined by Eqs. (67) and (68), in which the parameter G is fixed and the variable is the phase frequency ω .

A characteristic feature of the curves $R(\varepsilon, \omega)$ and $T(\varepsilon, \omega)$ in Fig. 3 is their resonance behaviour in the thin-wall regime as the phase frequency $\omega \to \omega_{\rm tn} = 1/4$. Specifically, we can see that the curve $R(\varepsilon, 0.250001)$ vanishes at $\varepsilon \approx 0.655$. Accordingly, the curve $T(\varepsilon, 0.250001)$ tends to unity at this point. To better describe the resonance behaviour of the curves $R(\varepsilon, \omega)$ in the thin-wall regime, Fig. 4 illustrates the dependence of the product $\tilde{R}(\varepsilon, \omega) = \exp(6.74\varepsilon)R(\varepsilon, \omega)$ on the parameter ε . The curves $\tilde{R}(\varepsilon, \omega)$ correspond to two values of the phase frequency ω in the close vicinity of the thin-wall limit $\omega_{\rm tn} = 1/4$. The exponential factor $\exp(6.74\varepsilon)$ was selected empirically. It is necessary to compensate for a decrease in $R(\varepsilon, \omega)$ with an increase in ε . It follows from Fig. 4 that there is an infinite sequence of points ε_k such that $R(\varepsilon_k) = 0$. As k increases, the difference $\Delta \varepsilon_k = \varepsilon_k - \varepsilon_{k-1}$ increases slightly and tends to a constant limit $\Delta \varepsilon$. This limit depends on the phase frequency ω , and decreases as $\omega \to \omega_{\rm tn}$. Hence, the distance between the successive zeros of R decreases with an increase in the size of the Q-ball. The successive zeros of R are separated by peaks. It follows from Fig. 4 that the height of these peaks decreases exponentially with an increase in ε .

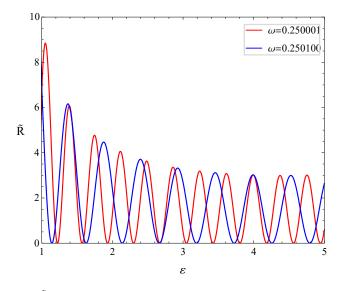


Fig. 4. Dependence of the product $\tilde{R} = \exp(6.74\varepsilon)R$ on the energy parameter ε for two values of the phase frequency of the Q-ball. The curves correspond to the parameters h = 0.2 and G = 0.2.

The resonance behaviour of the curves shown in Figs. 3 and 4 can be explained at a qualitative level. Due to its non-topological nature, the one-dimensional Q-ball has two boundary regions. As $\omega \to \omega_{\rm tn}$ (the thin-wall regime), the spatial size of the one-dimensional Q-ball increases, representing a large homogeneous central region bounded by two thin boundary regions. The process of transmission (reflection) of a fermion wave can occur at both the left and right boundaries of the Q-ball. When the incident fermionic wave falls on the left boundary of the Q-ball, part of it is reflected and the remainder passes into the interior of the Q-ball. Having reached the the right boundary of the Q-ball, part of the fermion wave is transmitted and leaves the Q-ball, and the reminder is reflected into the Q-ball. The reflected wave will then reach the left boundary of the Q-ball, where the process is repeated. Thus, the resulting reflected fermionic wave is determined by the superposition of multiple reflected waves. The zeros of R correspond to destructive wave interference, whereas its peaks correspond to constructive interference. The exponential decrease in the peak height of R with increasing ε occurs because the amplitude of each of the reflected fermionic waves also decreases exponentially as ε increases. Due to unitarity condition (56), the resonance behaviour of the reflection coefficient T. The situation is somewhat reminiscent of the passage of a light wave through an antireflection lens.

Figure 5 shows an Argand diagram for the elastic S-matrix elements $S_{1/2, 1/2}$ and the complex conjugate inelastic S-matrix elements $S_{-1/2, 1/2}^*$ for different values of the phase frequency ω . In contrast to Fig. 2, the intersection of the solid and dashed curves cannot be avoided in this case. In the same way as in Fig. 2, the solid curves start ($\varepsilon = 0$) and end ($\varepsilon \to \infty$) on the real axis, and tend to unity as $\varepsilon \to \infty$. This means that, as in Fig. 2, the difference in the phase shifts $\Delta = \delta(0) - \delta(\infty)$ of the elastic matrix elements $S_{1/2,1/2}$ is equal to zero over the entire allowable range of the phase frequency ω .

From Fig. 5 it follows that at $\varepsilon = 0$, the dashed curves, which correspond to the complex conjugate inelastic matrix elements $S_{-1/2,1/2}^*$, start on the imaginary axis. As $\omega \to \omega_{\rm tn}$ and $\varepsilon = 0$, the inelastic matrix elements tend to the point (0, -i) lying on the unitary circle. This corresponds to suppression of the elastic channel in the thin-wall regime at small ε , and agrees with the behaviour of the curves in Fig. 3. As ε increases, the matrix elements leave the imaginary axis and move along rather complex trajectories within the unitary circle. The smaller the difference $\delta = \omega - \omega_{\rm tn}$, the longer the dashed curve in the vicinity of the unitary circle. As $\varepsilon \to \infty$, the dashed curves tend to the origin. Furthermore, it follows from Fig. 5 that for $\omega = 0.251, 0.2501, 0.25001, and 0.250001$, the dashed curves self-intersect at the origin.

For greater clarity, Fig. 6 shows the behaviour of the dashed curve corresponding to $\omega = 0.250001$ in the neighbourhood of the origin. We can see that the dashed curve crosses the origin at least four times. In fact,

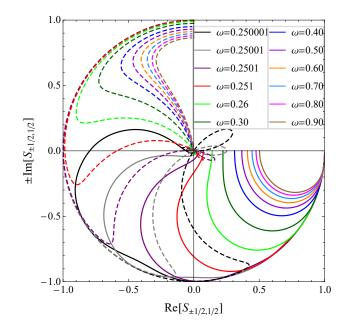


Fig. 5. Argand diagram for the S-matrix elements $S_{1/2, 1/2}$ (solid curves) and complex conjugate S-matrix elements $S_{-1/2, 1/2}^*$ (dashed curves) for different values of the phase frequency of the Q-ball. The curves correspond to the parameters h = 0.2 and G = 0.2.

from Fig. 4 it follows that the curve intersects the origin an infinite number of times, as the intersections of the origin correspond to the zeros of R in Fig. 4. These intersections, however, are indistinguishable since in Fig. 4, the height of the peaks of R decreases exponentially with an increase in ε . Note that according to the unitarity condition (56), the solid lines touch the unitary circle whenever the corresponding dashed lines cross the origin.

In the following, we present numerical results for the evaporation of the Q-ball. As in Sec. 4, when discussing this subject, we use dimensional quantities and denote the corresponding dimensionless analogues with a tilde. Figure 7 shows the dependence of the evaporation rate of the Noether charge Q of the Q-ball on the dimensionless Yukawa coupling constant $\tilde{G} = g^{-1/2}G$ for different values of the reduced Noether charge $\tilde{Q} = gm^{-2}Q$. Except for one case, the curves in Fig. 7 correspond to moderate values of \tilde{Q} at which the Q-ball begins to enter the thin-wall regime. The remaining curve corresponds to a significantly greater value of the reduced Noether charge $\tilde{Q} = 2 \times 10^3$. At this value of \tilde{Q} , the Q-ball is in a pronounced thin-wall regime. It was found that the $m^{-1}dQ/dt$ curves that correspond to the larger values of \tilde{Q} are practically indistinguishable from the black solid curve in Fig. 7, which can therefore be regarded as the limiting curve. From Fig. 7, it follows that as \tilde{G} increases, all the $m^{-1}dQ/dt$ curves tend to the limiting value $m^{-1} dQ/dt|_{\text{max}} \approx \tilde{\omega}_{\text{tn}}/\pi = 0.0796$ defined by Eq. (60). At the same time, as the reduced Noether charge \tilde{Q} increases, the $m^{-1}dQ/dt$ curves tend to the limiting curve in Fig. 7.

To better understand the limiting behaviour of the $m^{-1}dQ/dt$ curves, Fig. 8 shows these curves in the vicinity of the origin. Compared to Fig. 7, the curves in Fig. 8 correspond to larger \tilde{Q} , and thus their limiting behaviour is more pronounced. Using the thin-wall approximation, in which the x-dependent part of the profile functions in Eqs. (14a) and (14b) is replaced by a rectangular function, it can be shown that as $G \to 0$, the evaporation rate

$$dQ/dt \sim 8G^2 g^{-1} \left(m^2 - \omega_{\rm tn}^2\right) L,$$
(69)

where the linear size L of the Q-ball is related to its Noether charge Q by Eq. (63). It follows from Eq. (69) that the first derivative of the evaporation rate dQ/dt with respect to G vanishes at G = 0. The second derivative, however, is proportional to $L \approx Q/j_0$, and hence it increases indefinitely in the thin-wall regime when both L and Q tend to infinity.

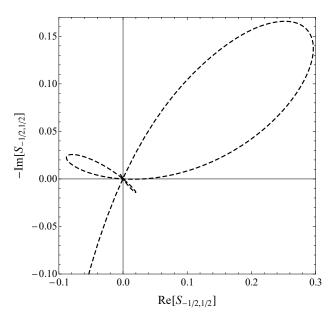


Fig. 6. Fragment of an Argand diagram for the complex conjugate S-matrix element $S^*_{-1/2, 1/2}$ in the vicinity of the origin. The curve corresponds to the parameters h = 0.2, G = 0.2, and $\omega = 0.250001$.

It follows from Fig. 8 that as $\tilde{Q} \to \infty$, the $m^{-1} dQ/dt$ curves degenerate into a limiting straight line in the vicinity of the origin. Using the thin-wall approximation, it can be shown that this limiting straight line is described by the expression

$$dQ/dt \approx \pi^{-1}G \left|\phi\left(0\right)\right| = 2^{3/2} \pi^{-1} G g^{-1/2} \left(m^2 - \omega_{\rm tn}^2\right)^{1/2}.$$
(70)

From Figs. 7 and 8, it follows that for $\tilde{Q} \gtrsim 200$, the shape of the $m^{-1}dQ/dt$ curves practically ceases to depend on the magnitude of \tilde{Q} , and the reduced evaporation rate $m^{-1}dQ/dt$ is determined only by the value of the dimensionless Yukawa coupling constant $\tilde{G} = g^{-1/2}G$. In this case, the Noether charge of the Q-ball decreases linearly with time:

$$Q(t) \approx Q(0) - m\Gamma(\tilde{G})t, \tag{71}$$

where $\Gamma(\tilde{G})$ is the limiting $m^{-1}dQ/dt$ curve shown in Figs. 7 and 8. It follows that the evaporation of the Noether charge results in a finite lifetime of the Q-ball, $\tau \approx Q/(m\Gamma(\tilde{G})) \geq \pi Q \omega_{\text{tn}}^{-1}$. We see that the lifetime of the Q-ball τ is $\propto Q$, and can therefore be arbitrarily large in the thin-wall regime since $\lim_{\omega \to \omega_{\text{tn}}} Q(\omega) = \infty$.

This is possible because in the thin-wall regime, the evaporation of the Q-ball occurs only at its boundaries rather than within its interior. In the latter case, the decrease in the charge would be exponential rather than linear, meaning that the lifetime of the Q-ball would not depend on the magnitude of its charge.

6. Conclusion

In the present paper, we study the scattering of massless fermions in the background field of a onedimensional Q-ball. Since the one-dimensional Q-ball solution is known in analytical form, we were able to obtain analytical expressions for the fermionic wave functions in terms of the local Heun functions. The analytical form of the fermionic wave functions makes it possible to derive general analytical expressions for the transmission coefficient T, reflection coefficient R, and corresponding S-matrix elements. In turn, the existence of these general expressions greatly simplifies the numerical study of the properties of fermion-Qball scattering.

The main feature of fermion-Q-ball scattering is the resonance behaviour of the transmission and reflection coefficients in the thin-wall regime. This resonance behaviour consists of the existence of an infinite

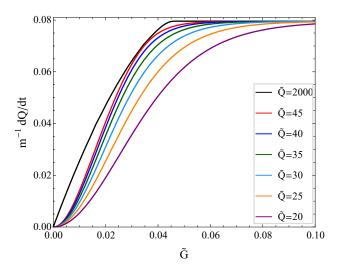


Fig. 7. Dependence of the evaporation rate of the Noether charge Q of the Q-ball on the dimensionless Yukawa coupling constant $\tilde{G} = g^{-1/2}G$ for different values of the reduced Noether charge $\tilde{Q} = gm^{-2}Q$. The curves correspond to the dimensionless parameter $\tilde{h} = m^2 g^{-2} h = 0.2$.

sequence of values ε_i of the energy parameter, such that $R(\varepsilon_i) = 0$ and $T(\varepsilon_i) = 1$. The zeros of the reflection coefficient R are separated by peaks whose height decreases exponentially with an increase in their sequence number. The reason for the resonance behaviour of the coefficients R and T is due to the nontopological nature of the Q-ball, resulting in the existence of two boundary regions for the one-dimensional Q-ball. The existence of these two boundaries makes possible multiple reflections of fermionic waves inside the Q-ball. The resonance structure of the coefficient R (T) results from the interference of these multiple reflected waves at the left (right) boundary of the Q-ball.

Unlike a one-dimensional Q-ball, a kink is a one-dimensional topological soliton. The kink interpolates between two topologically different vacua, and essentially consists of a single transition region. This makes the multiple reflection of waves impossible in fermion-kink scattering. As a result, the energy dependence of the transmission and reflection coefficients has no resonance structure in this case.

The Q-ball solution is $\propto \exp(-i\omega t)$, and hence has a nontrivial time dependence. As a result, the energy of fermions is not conserved when they are reflected in the background field of the Q-ball. Moreover, when the energy parameter $\varepsilon \in (-\omega/2, \omega/2)$, it becomes possible to produce fermion-antifermion pairs that carry away the energy and Noether charge of the Q-ball [34, 36, 37]. In the thin-wall regime, the Noether charge, energy, and linear size of the Q-ball become large, and the one-dimensional Q-ball has a spatially homogeneous distribution of energy and charge except for two thin boundary regions. In this case, pair production cannot occur in the interior of the Q-ball, and is possible only at its boundaries. Pair production results in the evaporation of the Noether charge, leading to a decrease in the linear size of the Q-ball.

In the leading order of the semi-classical approximation, the evaporation rate of the Noether charge can be expressed in terms of the integral of the reflection coefficient R over the region $\varepsilon \in (-\omega/2, \omega/2)$. In our case, the condition for the applicability of the semi-classical approximation is the smallness of the dimensionless combination gm^{-2} at fixed values of the other dimensionless combinations. We studied the dependence of the evaporation rate dQ/dt on the dimensionless Yukawa coupling constant $\tilde{G} = g^{-1/2}G$ for a number of values of the reduced Noether charge $\tilde{Q} = gm^{-2}Q$, and found that the $m^{-1}dQ/dt$ curves tend to a limiting curve as $\tilde{Q} \to \infty$. As \tilde{G} increases, this limiting curve tends to the limiting value $\omega_{\rm tn}/(\pi m)$, which depends only on the dimensionless combination $\tilde{h} = m^2 g^{-2}h$.

It follows from the results presented in this work that in the thin-wall regime, the character of the fermion-Q-ball interaction is determined by two parameters: the phase frequency ω and the parameter $\varepsilon_{1/2}$ defined in Eq. (68). There are two possible cases: $\omega/2 < \varepsilon_{1/2}$ and $\omega/2 > \varepsilon_{1/2}$. In the first case, if the energy parameter $\varepsilon \in (-\omega/2, \omega/2)$, then evaporation of the Q-ball takes place, if $\omega/2 < \varepsilon \leq \varepsilon_{1/2}$, then almost all of

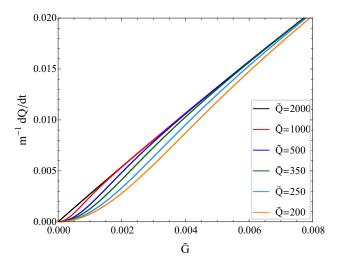


Fig. 8. Dependence of the evaporation rate of the Noether charge Q of the Q-ball on the dimensionless Yukawa coupling constant $\tilde{G} = g^{-1/2}G$ for different values of the reduced Noether charge $\tilde{Q} = gm^{-2}Q$. The curves correspond to the dimensionless parameter $\tilde{h} = m^2 g^{-2} h = 0.2$.

the incident fermions are reflected from the Q-ball, and if $\varepsilon \gtrsim \varepsilon_{1/2}$, then almost all of the incident fermions pass through the Q-ball. In the second case, if the energy parameter $\varepsilon \in (-\omega/2, \omega/2)$, then evaporation of the Q-ball takes place as in the first case, and if $\varepsilon > \omega/2$, then almost all of the incident fermions pass through the Q-ball. We see that if $\omega/2 > \varepsilon_{1/2}$, then reflection of fermions is practically absent.

A characteristic property of fermion-Q-ball scattering is that the parameter $\varepsilon_{1/2}$ is approximately equal to the effective mass $m_{\psi,\text{eff}}$ of the fermion in the background field of the Q-ball. In turn, the effective mass $m_{\psi,\text{eff}} \approx 3^{1/2} 2^{-1} \tilde{G} \tilde{h}^{-1/2} m$. In the semi-classical regime, the dimensionless coupling constants $\tilde{G} = g^{-1/2} G$ and $\tilde{h} = m^2 g^{-2} h$ are ≤ 1 . It follows that in this regime, the effective fermion mass $m_{\psi,\text{eff}} \leq m$, where m is the mass of the scalar boson. We see that in the semi-classical regime, the mass of the scalar boson significantly affects the character of fermion-Q-ball scattering.

References

- [1] T. D. Lee, Y. Pang, Phys. Rep. 221 (1992) 251.
- [2] E. Radu, M. Volkov, Phys. Rep. 468 (2008) 101.
- [3] N. Manton, P. Sutcliffe, Topological Solitons, Cambridge University Press, Cambridge, 2004.
- Y. M. Shnir, Topological and Non-Topological Solitons in Scalar Field Theories, Cambridge University Press, Cambridge, 2018.
- [5] G. Rosen, J. Math. Phys. (N.Y.) 9 (1968) 996.
- [6] S. Coleman, Nucl. Phys. B 262 (1985) 263.
- [7] A. Safian, S. Coleman, M. Axenides, Nucl. Phys. B 297 (1988) 498.
- [8] A. Safian, Nucl. Phys. B 304 (1988) 403.
- [9] G. Rosen, J. Math. Phys. (N.Y.) 9 (1968) 999.
- [10] K. Lee, J. A. Stein-Schabes, R. Watkins, L. M. Widrow, Phys. Rev. D 39 (1989) 1665.
- [11] C. H. Lee, S. U.Yoon, Mod. Phys. Lett. A 6 (1991) 1479.
- [12] K. N. Anagnostopoulos, M. Axenides, E. G. Floratos, N. Tetradis, Phys. Rev. D 64 (2001) 125006.
- [13] T. S. Levi, M. Gleiser, Phys. Rev. D 66 (2002) 087701.
- [14] H. Arodz, J. Lis, Phys. Rev. D 79 (2009) 045002.
- [15] V. Benci, D. Fortunato, J. Math. Phys. (N.Y.) 52 (2011) 093701.
- [16] T. Tamaki, N. Sakai, Phys. Rev. D 90 (2014) 085022.
- [17] I. E. Gulamov, E. Y. Nugaev, M. N. Smolyakov, Phys. Rev. D 89 (2014) 085006.
- [18] Y. Brihaye, V. Diemer, B. Hartmann, Phys. Rev. D 89 (2014) 084048.
- [19] J. Hong, Y. Kim, P. Y. Pac, Phys. Rev. Lett. 64 (1990) 2230.
- [20] I. E. Gulamov, E. Y. Nugaev, A. G. Panin, M. N. Smolyakov, Phys. Rev. D 92 (2015) 045011.
- [21] A. Yu. Loginov, V. V. Gauzshtein, Phys. Rev. D 102 (2020) 025010.
- [22] A. Kusenko, Phys. Lett. B 405 (1997) 108.

- [23] A. Kusenko, M. Shaposhnikov, P. Tinyakov, Pis'ma Zh. Exp. Teor. Fiz. 67 (1998) 229.
- [24] K. Enqvist, J. McDonald, Phys. Lett. B 425 (1998) 309.
- [25] G. Dvali, A. Kusenko, M. Shaposhnikov, Phys. Lett. B 417 (1998) 99.
- [26] A. Kusenko, M. Shaposhnikov, Phys. Lett. B 418 (1998) 46.
- [27] K. Enqvist, J. McDonald, Nucl. Phys. B 538 (1999) 321.
- [28] S. Kasuya, M. Kawasaki, Phys. Rev. D 61 (2000) 041301.
- [29] K. Enquist, A. Mazumdar, Phys. Rep. 380 (2003) 99.
- [30] A. Kamada, M. Kawasaki, M. Yamada, Phys. Lett. B 719 (2013) 9.
- [31] S. Kasuya, M. Kawasaki, M. Yamada, Phys. Lett. B 726 (2013) 1.
- [32] E. Cotner, A. Kusenko, Phys. Rev. Lett. 119 (2017) 031103.
- [33] E. Cotner, A. Kusenko, Phys. Rev. D 96 (2017) 103002.
- [34] A. G. Cohen, S. R. Coleman, H. Georgi, A. Manohar, Nucl. Phys. B 272 (1986) 301.
- [35] A. V. Kovtun, E. Y. Nugaev, Mod. Phys. Lett. A 32 (2017) 1750198.
- [36] T. Multamaki, I. Vilja, Nucl. Phys. B 574 (2000) 130.
- [37] S. S. Clark, Nucl. Phys. B 756 (2006) 38.
- [38] A. Kusenko, Phys. Lett. B 404 (1997) 285.
- [39] F. P. Correia, M. Schmidt, Eur. Phys. J. C 21 (2001) 181.
- [40] A. Ronveaux (Ed.), Heun's differential equations, Oxford University Press, Oxford, 1995.
- [41] F. W. J. Olver, D. W. Lozier, R. F. Boisvert, C. W. Clark (Eds.), NIST Handbook of Mathematical Functions, Cambridge University Press, Cambridge, 2010.
- [42] L. D. Landau, E. M. Lifshitz, Quantum Mechanics: Non-Relativistic Theory. Vol. 3 (3rd ed.), Pergamon Press, Oxford, 1977.
- [43] M. L. Goldberger, K. M. Watson, Collision Theory, John Wiley & Sons, New York, 1967.
- [44] J. R. Taylor, Scattering Theory: Quantum Theory on Nonrelativistic Collisions, John Wiley & Sons, New York, 1972.